Material Property Changes in Defects Caused by Reverse Bias Exposure of CIGS Solar Cells

Bakker, Klaas; Åhman, Hanna Nilsson; Aantjes, Kees ; Barreau, Nicolas; Weeber, Arthur; Theelen, Mirjam

DOI
10.1109/JPHOTOV.2019.2940486

Publication date
2019

Document Version
Accepted author manuscript

Published in
IEEE Journal of Photovoltaics

Material property changes in defects caused by reverse bias exposure of CIGS solar cells

Klaas Bakker, Hanna Nilsson Åhman, Kees Aantjes, Nicolas Barreau, Arthur Weeber and Mirjam Theelen

***Abstract*— Partial shading of $Cu(In,Ga)Se_2$ modules can lead to the formation of reverse bias induced wormlike defects. These wormlike defects act as local shunts and permanently decrease module output. A good understanding of the formation and propagation mechanisms of these defects is needed in order to mitigate the negative effects, or to prevent these defects from forming. In this study wormlike defects were formed on small non encapsulated cells by exposing them to reverse bias conditions. SEM-EDX measurements showed a rearrangement of elements: indium, gallium and copper were replaced by cadmium while selenium was replaced by sulfur in the area around the defect. Moreover, additional electronic-defect levels were found in that area with spectrally resolved photoluminescence spectroscopy. Based on the material changes in the area close to the wormlike defects, a propagation mechanism is proposed. The model assumes a chemical reaction as the driving force for propagation instead of melting due to ohmic heating.**

***Index Terms*—Cadmium, Electric breakdown, Photoluminescence, Photovoltaic cells, Reliability, Thin film devices.**

I. Introduction

Partial shading of $Cu(In,Ga)Se_2$ (CIGS) PV modules can result in potential harmful reverse bias conditions in the shaded region of the PV module. Reverse bias is the common term used for the negative (or reverse) operating voltage of the shaded cells in a partly shaded PV module. This operating condition is a consequence of the electrical series connection of all cells in a PV module. Due to the series connection the photocurrent of the non-shaded cells is forced through the shaded cells. This surplus of electric current results in the dissipation of energy within the shaded cell. This reverse flow of energy can result in the formation of reverse bias induced defects. These defects permanently decrease the output of the PV module. More defects can be created after consecutive shading events [1]. Shading, and the formation of reverse bias induced defects, can therefore have a negative effect on the long term stability and operation in the field [2].

During shading events in both CIGS and CdTe local hotspots occur that can propagate within a cell [3]. The local hotspot leaves defects behind that act as local shunts. The difference between CdTe and CIGS is that in CIGS the defects leaves trails that show an unique visual patterns [4] and are therefore often referred to as wormlike defects. Wormlike defects in CIGS have been observed in both packaged and unpackaged [5] CIGS devices. The composition of the absorber changes at the CIGS – TCO interface. The CIGS material expands and gets more porous [6]. This expanded porous material underneath the TCO film gives the wormlike defects its typical visual appearance. The structural appearance of wormlike defects have been described in detail [4]–[6]. However, the propagation mechanism of these defects is still unclear. In this study, a propagation mechanism for these wormlike defects is presented based on compositional changes found at the edge of wormlike defects.

II. Materials And Methods

10 non-encapsulated small cells with an active area of approximately 5 mm x 7 mm were used. The layout of these cells is specifically designed to mimic the geometry in a monolithically interconnected module, including analogues for the P1 and P3 interconnection scribes. The layer stack of the CIGS solar cells used is: 1mm soda-lime glass, 500 nm DC-sputtered molybdenum, 2 µm coevaporated CIGS, 50 nm chemical bath deposited cadmium sulfide, 65 nm DC sputtered intrinsic zinc oxide, 1 or 2 µm DC sputtered aluminum doped zinc oxide and 60 nm thermally evaporated gold contacts to the sides. A detailed description of the cell design and fabrication procedure can be found in [7].

In order to simulate partial shading in a module, which can results in the formation of wormlike defects, a reverse bias treatment was performed by sweeping a voltage in the dark from +0.7 till -10.0 Volt, using a Keithley 2400 source measure unit that was controlled by Tracer 3 software. Further analysis with Scanning Electron Microscopy - Energy Dispersive X-ray spectroscopy (SEM – EDX), spectrally resolved photoluminescence (sr-PL) and spatially resolved photoluminescence (PL) were performed with a JEOL JSM-6010LA IntouchScope, Horiba Labram Aramis Raman microscope equipped with a Symphony IR detector and a 532nm laser and a Greateyes LumiSolarCell LED based EL/PL system respectively. All instrument settings were kept constant throughout the experiment except for the

This paragraph of the first footnote will contain the date on which you submitted your brief for review. This work is supported by 'Netherlands Enterprise Agency' (RvO) and the Dutch Topteam Energy via the projects: 'Building Integrated PhotoVoltaic Panels on Demand - in The Netherlands' with grant number TEID215005 and 'Performance and Electroluminescence Analysis on Reliability and Lifetime of Thin-Film Photovoltaics' with grant number TEUE116203. Furthermore, the Early Research Program 'Sustainability & Reliability for solar and other (opto-)electronic thin-film devices' from TNO is also acknowledged for funding.

Klaas Bakker is both with the PVMD group at Delft university of Technology, Mekelweg 4, 2628 CD Delft. The Netherlands and with ECN part of TNO - Solliance, High Tech Campus 21, 5656 AE Eindhoven, The Netherlands

Hanna Nilsson Åhman, Kees Aantjes and Mirjam Theelen are with ECN part of TNO - Solliance, High Tech Campus 21, 5656 AE Eindhoven, The Netherlands.

Nicolas Barreau is with the Institut des Matériaux Jean Rouxel of the Université de Nantes, 2 rue de la Houssinière, BP 32229, 44322 Nantes Cedex 3 France.

Arthur Weeber is both with the PVMD group at Delft university of Technology, Mekelweg 4, 2628 CD Delft. The Netherlands and with ECN part of TNO - Solar Energy, Westerduinweg 3, 1755 LE Petten, The Netherlands.

integration time used during sr-PL measurement, this varied between 1 and 3 seconds dependent on signal strength. SEM-EDX measurements were performed at acceleration voltages of both 6 and 18kV, the results of EDX point analyses are always the average of 8 measurements.

In order to perform different analyses on the samples after formation of wormlike defect an etching procedure was used. Fig. 1 schematically shows the etching procedure, after the first step sr-PL measurements were performed while SEM-EDX measurements were done after the second step. In order to allow for sr-PL the conductivity of the Al:ZnO needs to be interrupted, while leaving a thin layer of ZnO and CdS to protect the CIGS absorber material from photo-degradation during sr-PL measurements. This was accomplished by carefully removing the Al:ZnO with acetic acid. The sample was etched in several sessions of 30 seconds, checking the progress with PL after each session until the full non-degraded area exhibits a bright PL signal. In order to allow for EDX measurements on the bare absorber a second etching step using 3 wt.% hydrochloric acid (HCl) was performed after the sr-PL measurements. The etch time for this final step was determined based on preliminary experiments. These experiments showed complete removal of CdS after 5 minutes in 3 wt.% HCl on the non-degraded parts. In this study an etch time of 15 minutes was used in order to account for possible differences in etch rate in the degraded area.

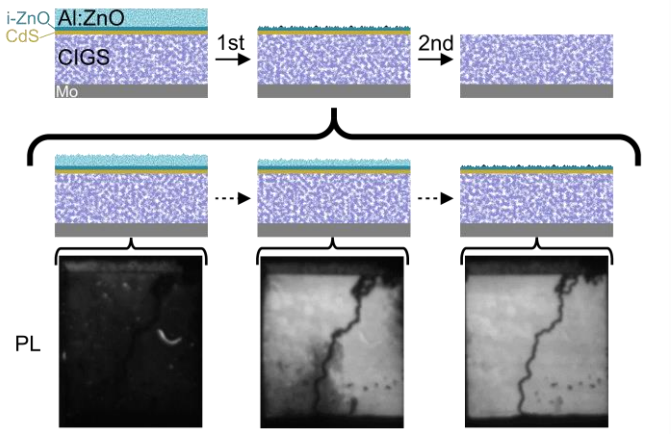

Fig. 1 Schematic of etching procedure. First etching step is to allow for sr-PL measurements. During the first step the conductive Al:ZnO is removed with acetic acid, checking after every 30 seconds etch, with PL, until the full non-degraded area exhibits a bright PL signal. Second step is removal of the residual ZnO and CdS with hydrochloric acid to obtain a clean surface for SEM – EDX.

III. Results And Discussion

A. Defect creation and appearance

The reverse bias treatments resulted in the formation of wormlike defects in 8 out of the 10 samples. For the 8 defected samples the average efficiency was reduced from 12.4 ± 0.8% to 0.4 ± 0.6% . Moreover for 6 out of these 8 cells the shunting was so severe that the electrical output was reduced to 0% [8].

Fig. 2 shows a microscope image of the surface of a severely shunted cell after reverse bias treatment. In this figure, wormlike defects can be observed in the form of white meandering lines. Confocal microscopy shows that wormlike defects consist of small individual protruding mountains that are linked together (Fig. 3). No

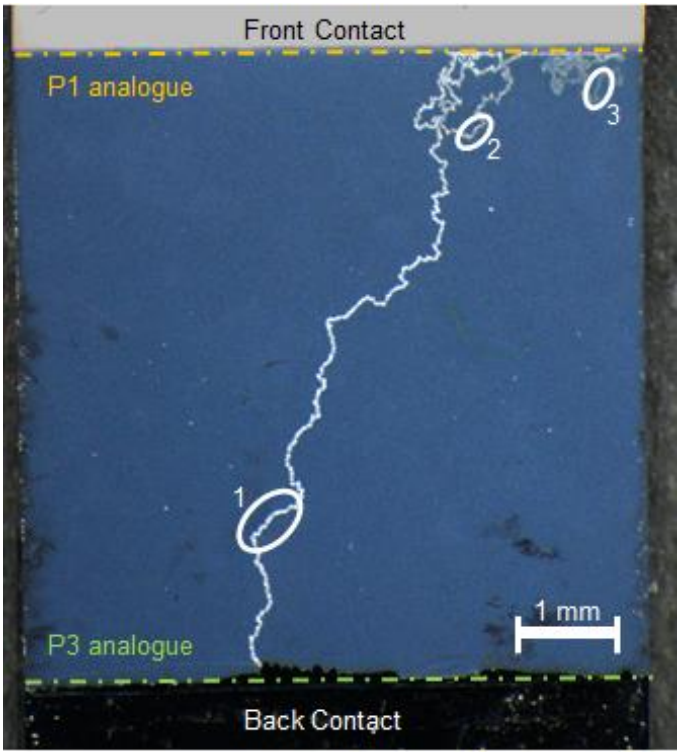

Fig. 2 Microscope image of a cell with wormlike defects. Dashed lines indicate the positions of the P1 and P3 scribe analogues. Numbered red circles indicate different sizes of wormlike defects.

major differences were observed in confocal microscopy before and after etching. Furthermore Fig. 2 displays apparent differences in the brightness of the trails, indicated by the numbered red circles. Brighter trails (number 1) are wider and are made up of bigger individual islands than the darker trails (number 2 and 3) [8]. In addition, the trails seem to propagate along a line at the top of the picture. This line is indicated with a dashed orange line in Fig. 2 and coincides with the P1 analogue, which is the border of the molybdenum layer underneath the solar cell. For all cells where the wormlike defects reached the P1 analogue the efficiency was reduced to 0%.

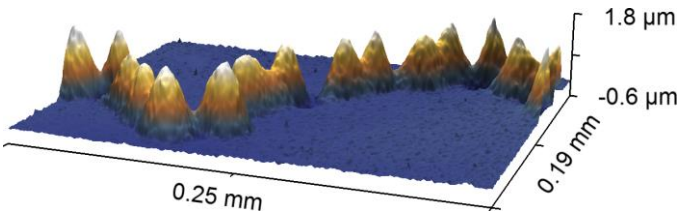

Fig. 3 Confocal microscopy image of a wormlike defect (before etching).

B. SEM EDX

The SEM image of Fig. 4 shows the bare CIGS material and the wormlike defect after the HCl etch. Inside the wormlike defect the material is changed into a porous material. The border region of the wormlike defect appears darker compared to the surrounding CIGS material, indicating that the material close to the defect differs from the bulk material further from the wormlike defect.

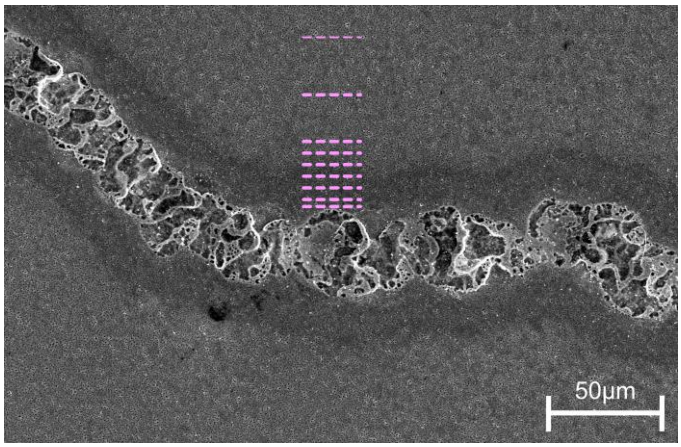

Fig. 4 Top view SEM image of wormlike defect after HCl etch. The pink dashed lines indicate the approximate position of the EDX point measurements.

EDX mapping showed changes in elements in this darker border region. To obtain more quantitative information on the changes in this border region a number of EDX point analysis have been performed. Even though the EDX is not calibrated it is able to visualize trends compared to measurements performed on the bulk material taken millimeters away from the affected area. The results of the EDX measurements are shown in Fig. 5. The values on the y-axis are in atom percent and are deviations from the bulk measurements. Furthermore all datapoints are an average of eight measurements. Repeating the measurement process on different locations on the same sample yielded comparable results. Furthermore the data shown was obtained with an acceleration voltage of 6kV to probe close to the surface of the material. Table I lists the EDX deviations from the bulk for Cd and S for two different acceleration voltages. From the table it can be observed that measurements with a higher penetration depth, performed at 18 kV, showed the same trend however the deviations from bulk measurements were much smaller. This indicates that the observed changes mostly take place at the surface of the material.

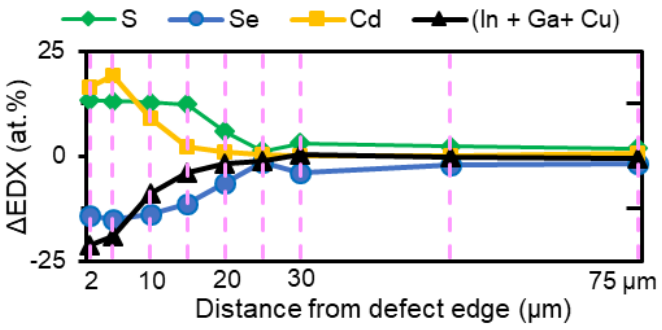

Fig. 5 EDX Deviation from bulk measurements with respect to distance from the edge of the wormlike defect. EDX measurements were performed with at an acceleration voltage of 6kV. The EDX results on the y axis are in atom percent and are subtracted from the bulk measurements far away from the degraded area. The vertical pink dashed lines correspond with positions along the pink dashed lines of Fig. 4 where the measurements were performed.

TABLE I
AVERAGE ΔEDX VALUES FOR CADMIUM AND SULFUR ON THE MEASUREMENT POSITIONS INDICATED WITH PINK LINES IN FIG. 4

Position [µm]	ΔEDX (at%) Cd 6kV	ΔEDX (at%) Cd 18kV	ΔEDX (at%) S 6kV	ΔEDX (at%) S 18kV
Bulk	0.0	0.0	0.0	0.0
75	0.6	0.1	2.0	0.3
50	0.2	0.4	2.4	0.7
30	0.2	0.2	3.2	0.3
25	0.5	0.0	1.3	0.6
20	1.2	0.2	5.9	0.8
15	2.2	0.8	12.3	2.3
10	8.9	3.5	12.8	3.3
5	19.3	4.4	13.2	3.2
2	16.6	5.8	13.4	3.5

From Fig. 5 it can be observed that the composition started to change around 25 µm from the edge of the defect, this coincides with the darker border region of the defect in Fig. 4. This change seems to occur in two separate processes:

1. The exchange of selenium for sulfur: Moving towards the defect, there is a simultaneous rise in sulfur content and a decline in selenium content that starts around 25 µm from the edge of the defect.
2. Indium, gallium and copper are likely replaced by cadmium. The presence of cadmium is surprising, since etching with HCl is expected to result in complete removal of the cadmium sulfide layer. Therefore, it is likely that the cadmium is incorporated in the modified absorber material.

The onset of the second process occurs closer to the edge of the defect, therefore it is likely that two separate processes are taking place.

In Table II the signals of Cu, In and Ga from Fig. 5 are listed and compared with the Cd signal. The decrease in the total (Cu + In + Ga) content appears similar to the increase in Cd content. It should be noted that the decrease in the copper signal only appears in close vicinity of the defect, further away there is even a slight surplus of copper. In contrast to the indium and gallium content that are reduced in a large area around the defect.

TABLE II
AVERAGE ΔEDX IN ATOM PERCENT FOR CD, (IN + GA + CU), IN, GA AND CU ON THE MEASUREMENT POSITIONS INDICATED WITH PINK LINES IN FIG. 4

Position [µm]	ΔEDX Cd	ΔEDX (In+Ga+Cu)	ΔEDX In	ΔEDX Ga	ΔEDX Cu
Bulk	0.0	0.0	0.0	0.0	0.0
75	0.6	-0.5	-1.1	0.0	0.6
50	0.2	0.0	-1.0	0.0	1.0
30	0.2	0.4	-0.7	-0.7	1.8
25	0.5	-1.1	-0.9	-1.2	1.0
20	1.2	-1.8	-2.2	-1.3	1.7
15	2.2	-3.7	-5.7	-2.1	4.0
10	8.9	-8.9	-8.2	-1.9	1.2
5	19.3	-19.0	-12.2	-2.6	-4.3
2	16.6	-21.1	-8.5	-4.9	-7.7

Cd is known to diffuse into CIGS under the influence of temperature [9]. A recent study by Biderman et al. [10] ruled out the diffusion by grain boundaries. Reference [10] suggested that the Cd diffusion process is a combination of both substitutional-vacancy based diffusion and interstitial based diffusion. For both mechanisms a Cd ion reacts with a vacancy to form substitutional cadmium (Cd_{Cu}, Cd_{In} or Cd_{Ga}). In the case of the substitutional-vacancy based diffusion process the substitutional Cd jumps to a neighboring vacancy. In an interstitial based diffusion process the Cd ion diffuses through the lattice as an interstitial and reacts with a vacancy.

Furthermore Biderman et al. [10] stated that the Cd ions preferred to occupy copper vacancies. The results from this experiment however suggest that during reverse bias induced defect formation the Cd is mostly replacing In and Ga. Possibly In and Ga and to a lesser extend Cu, during defect formation, migrate from the border region leaving vacancies that are occupied by Cd ions, supplied from the CdS buffer layer. It is likely that the missing elements have migrated from the border region to the wormlike defect.

C. Spectrally resolved Photoluminescence spectroscopy

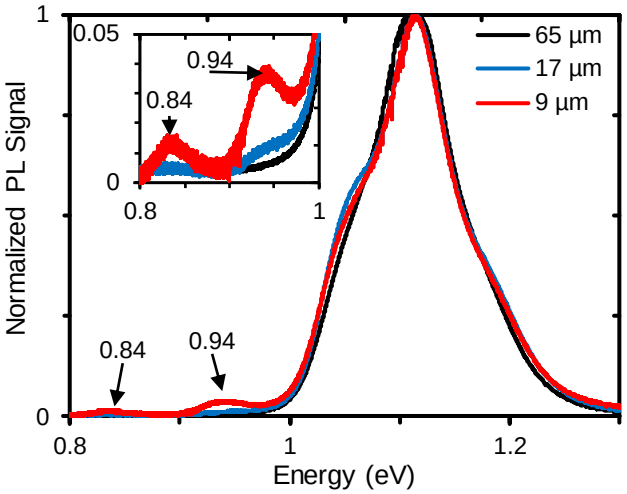

Fig. 6 Normalized PL spectra obtained at different distances from the edge of the defect. The inset shows a magnification of the region between 0.8 and 1.0 eV.

Fig. 6 shows normalized PL spectra obtained at several positions in the border region of the defect. Compared to the measurement in the bulk (65 µm distance), two additional features were found in PL spectra measured closer to the defect (9 and 17 µm). The peak position of these additional features are not constant between samples and on different positions within one same sample, and are within the range of 0.84 - 0.87 eV and 0.94 - 0.97 eV. Peaks at lower energies are usually assigned to energy transitions between donor-acceptor pairs between different point defects, vacancies, interstitials and substitutional-vacancies. A peak around 0.94 eV has been described and some of the literature have assigned the peak around 0.94 eV to Cd_{Cu} [11], [12]. Although the exact nature of the peaks is unknown, substitutional cadmium could be a possibility due to the large amount of Cd found in the EDX measurements. Therefore these peaks are assigned to the presence of cadmium. In Fig. 7 the contribution of cadmium is expressed as the ratio between the areas of the 0.84 eV and 0.94 eV peaks and the area of the total spectrum. As can be observed from Fig. 7, the onset of the Cd PL contribution takes place on the same distance scale as the compositional changes observed in the EDX measurement.

Inside the wormlike defect no PL signal could be measured. Close to the edge of the defect, PL spectra could be obtained however with a much lower intensity compared to the unaffected bulk material. In general a decrease in PL intensity is associated with a reduction of the local voltage and associated solar cell performance. Since there is a PL signal generated in the border region the semiconductor material properties in that area are not completely lost. However it is not yet possible to estimate the contribution of the deteriorated border region on the total shunt resistance of the defect.

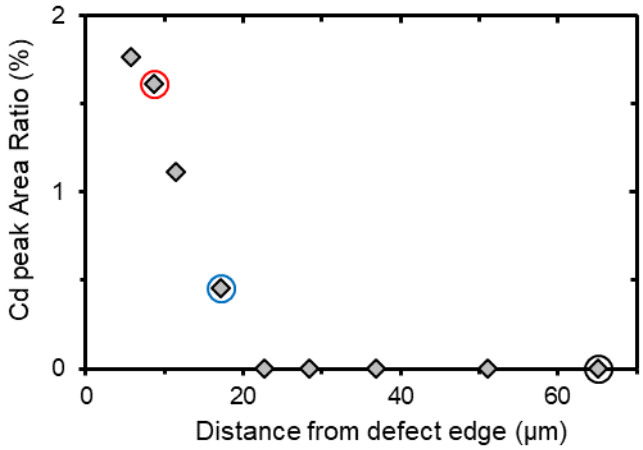

Fig. 7 Contribution of the Cd peak area Ratio from sr-PL as function of distance from the edge of the defect. The cadmium ratio is the area of the peaks at 0.84 eV and 0.94 eV divided by the area of the whole spectrum. The circled datapoints are the measurements displayed in Fig. 6.

D. Discussion on propagation mechanism

Based on the compositional changes in the edge observed by both EDX and sr-PL measurements a mechanism for worm formation and propagation is proposed. The proposed mechanism is based on the hypothesis that a (chemical) reaction is responsible for the observed compositional changes inside the wormlike defect. This reaction is fueled by the heat caused by the high current density in the defect. Reactants supplied from the surrounding region are required to sustain the growth of the defect. In order to get the reaction started heat, electricity and defected absorber material are probably needed simultaneously.

Fig. 8 displays a schematic of the propagation mechanism. In this proposed propagation model the formation and propagation goes through the following steps:

0. Start at a small weak spot (e.g. a shunt).
1. The small weak spot becomes a local hotspot during reverse bias operation as it conducts more current than the surrounding area.
2. A reaction starts that changes the material inside the defect to the more porous composition. Reactants for the reaction are obtained from the surrounding area.
3. The defect expands and forms an “island”. The reactants that have left the border region leave vacancies that are filled up with elements from the buffer layer, creating a “Cd” rich region.
4. Multiple new weak spots are created in the Cd rich area, because of the reduced (electronic) material properties. One or a cluster of several of these newly formed weak spots form a new local hotspot where the conditions are favorable in order to start a new reaction site.
5 The process starts again at step 1 creating a new island and the old islands cools down as the reaction stops.

Since the wormlike defect appears to propagate in the direction of the P1 scribe, the origin of supplied electrical current, implicates that electricity plays an important role in the process. Since the reaction mostly takes place at the surface [6] and the fact that the Al:ZnO layer stays intact supports the idea that electricity supplied by the TCO is needed for the reaction. The influence of the electric field is the subject of ongoing investigations [8].

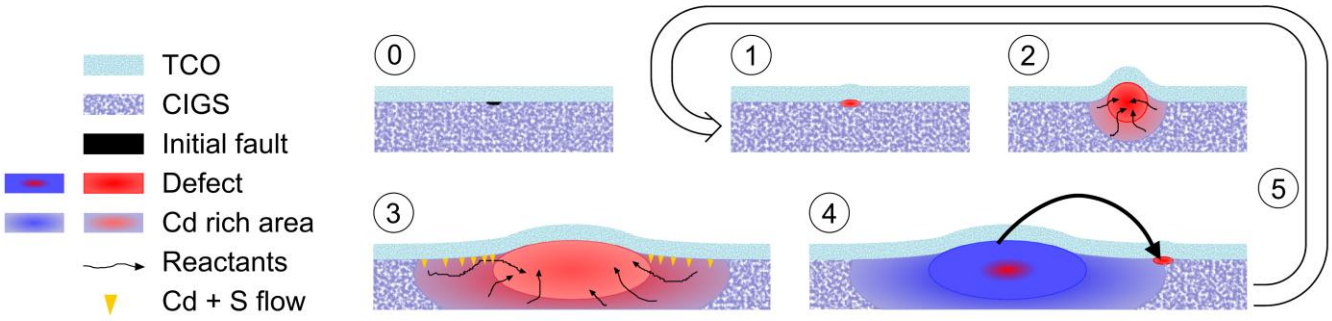

Fig. 8 Schematic of proposed propagation mechanism. Step 0 represents the initial starting point in the form of a local weak spot. In step 1, a reverse bias is applied and the weak spot becomes a hotspot. This hotspot expands in step 2 and start to attack reactants from the surrounding. In step 3 the defect has expanded and Cd and S from the buffer layer occupy the space left by the migrated reactants. In step 4 the hotspot shifts to a new location and the reaction starts again from the start in step 5.

Conclusions.

A propagation method was proposed based on the discrete islands that make up the wormlike defects and compositional changes found in the region next to the defects. The compositional changes in the region close to the defects originate at the surface and include the exchange of metals (Cu + In + Ga) for Cd from the buffer. Additional sr-PL measurements suggested that cadmium from the buffer layer is occupying vacancies left by the metals. For the proposed propagation method the wormlike defects starts at an initial weak spot. During reverse bias this weak spot becomes a local hotspot. Due to heat and an electric field a reaction is started in this hotspot. The hotspot expands and the reaction is partly fueled from material outside the wormlike defect. The hotspot moves to a next location because the original hotspot runs out of fuel and favorable conditions are created in the area of the new hotspot. This study revealed additional research questions. The two most prominent examples are, firstly the exact mechanism of the reaction inside the hotspot. Secondly the role of the electric field in the propagation of the wormlike defects. Both topics are subject of ongoing investigations.

References

[1] T. J. Silverman and I. Repins, “Partial Shade Endurance Testing for Monolithic Photovoltaic Modules,” in *2018 IEEE 7th World Conference on Photovoltaic Energy Conversion (WCPEC) (A Joint Conference of 45th IEEE PVSC, 28th PVSEC & 34th EU PVSEC)*, 2018, pp. 3932–3937.

[2] S. Wendlandt and L. Podlowski, “Influence of Near Field Shadowing on the Performance Ratio of Thin Film Modules,” in *35th European Photovoltaic Solar Energy Conference and Exhibition*, 2018, pp. 1230–1235.

[3] S. Johnston, D. Sulas, E. Palmiotti, A. Gerber, H. Guthrey, J. Liu, L. Mansfield, T. J. Silverman, A. Rockett, and M. Al-Jassim, “Thin-Film Module Reverse-Bias Breakdown Sites Identified by Thermal Imaging,” in *2018 IEEE 7th World Conference on Photovoltaic Energy Conversion (WCPEC) (A Joint Conference of 45th IEEE PVSC, 28th PVSEC & 34th EU PVSEC)*, 2018, no. d, pp. 1897–1901.

[4] P. O. Westin, U. Zimmermann, L. Stolt, and M. Edoff, “Reverse Bias Damage in CIGS Modules,” in *24th European Photovoltaic Solar Energy Conference*, 2009, pp. 2967–2970.

[5] E. Palmiotti, S. Johnston, A. Gerber, H. Guthrey, A. Rockett, L. Mansfield, T. J. Silverman, and M. Al-Jassim, “Identification and analysis of partial shading breakdown sites in CuIn x Ga (1-x) Se 2 modules,” *Sol. Energy*, vol. 161, pp. 1–5, Feb. 2018.

[6] J. E. Lee, S. Bae, W. Oh, H. Park, S. M. Kim, D. Lee, J. Nam, C. Bin Mo, D. Kim, J. Yang, *et al.*, “Investigation of damage caused by partial shading of CuInxGa (1-x) Se 2 photovoltaic modules with bypass diodes,” *Prog. Photovoltaics Res. Appl.*, vol. 24, no. 8, pp. 1035–1043, 2016.

[7] M. Theelen, K. Bakker, H. Steijvers, S. Roest, P. Hielkema, N. Barreau, and E. Haverkamp, “In Situ Monitoring of the Accelerated Performance Degradation of Solar Cells and Modules : A Case Study for Cu (In , Ga) Se 2 Solar Cells,” *J. Vis. Exp.*, vol. 140, no. October, 2018.

[8] K. Bakker, H. Nilsson Åhman, T. Burgers, N. Barreau, A. Weeber, and M. Theelen, “Propagation mechanism of reverse bias induced defects in Cu (In , Ga) Se 2 solar cells,” *Submitt. to Sol. Energy Mater. Sol. Cells*, 2019.

[9] S. Kijima and T. Nakada, “High-Temperature Degradation Mechanism of Cu(In,Ga)Se 2 -Based Thin Film Solar Cells,” *Appl. Phys. Express*, vol. 1, no. 7, p. 75002, Jun. 2008.

[10] N. J. Biderman, S. W. Novak, R. Sundaramoorthy, P. Haldar, and J. R. Lloyd, “Insights into cadmium diffusion mechanisms in two-stage diffusion profiles in solar-grade Cu(In,Ga)Se2thin films,” *Appl. Phys. Lett.*, vol. 107, no. 23, 2015.

[11] S. Shirakata, K. Ohkubo, Y. Ishii, and T. Nakada, “Effects of CdS buffer layers on photoluminescence properties of Cu(In,Ga)Se2 solar cells,” *Sol. Energy Mater. Sol. Cells*, vol. 93, no. 6–7, pp. 988–992, Jun. 2009.

[12] S.-H. Chen, W.-T. Lin, S.-H. Chan, S.-Z. Tseng, C.-C. Kuo, S.-C. Hu, W.-H. Peng, and Y.-T. Lu, “Photoluminescence Analysis of CdS/CIGS Interfaces in CIGS Solar Cells,” *ECS J. Solid State Sci. Technol.*, vol. 4, no. 9, pp. P347–P350, 2015.